

Gaussian Process-Based Bayesian Nonparametric Inference of Population Trajectories from Gene Genealogies

Julia A. Palacios and Vladimir N. Minin*
 Department of Statistics, University of Washington
 *corresponding author: vminin@uw.edu

Abstract

Changes in population size influence genetic diversity of the population and, as a result, leave a signature of these changes in individual genomes in the population. We are interested in the inverse problem of reconstructing past population dynamics from genomic data. We start with a standard framework based on the coalescent, a stochastic process that generates genealogies connecting randomly sampled individuals from the population of interest. These genealogies serve as a glue between the population demographic history and genomic sequences. It turns out that only the times of genealogical lineage coalescences contain information about population size dynamics. Viewing these coalescent times as a point process, estimating population size trajectories is equivalent to estimating a conditional intensity of this point process. Therefore, our inverse problem is similar to estimating an inhomogeneous Poisson process intensity function. We demonstrate how recent advances in Gaussian process-based nonparametric inference for Poisson processes can be extended to Bayesian nonparametric estimation of population size dynamics under the coalescent. We compare our Gaussian process (GP) approach to one of the state of the art Gaussian Markov random field (GMRF) methods for estimating population trajectories. Using simulated data, we demonstrate that our method has better accuracy and precision. Next, we analyze two genealogies reconstructed from real sequences of hepatitis C and human Influenza A viruses. In both cases, we recover more believed aspects of the viral demographic histories than the GMRF approach. We also find that our GP method produces more reasonable uncertainty estimates than the GMRF method.

1 Introduction

Statistical inference in population genetics increasingly relies on the coalescent (Kingman, 1982), the probability model that describes the relationship between a gene genealogy of a random sample of molecular sequences and effective population size. This model provides a good approximation to the distribution of ancestral histories that arise from classical population genetics models (Rosenberg and Nordborg, 2002). More importantly, coalescent-based inference methods allow us to estimate population genetic parameters, including population size trajectories, directly from genomic sequences (Griffiths and Tavaré, 1994). Recent examples of coalescent-based population dynamics estimation include reconstructing demographic histories of musk ox (Campos et al., 2010) from fossil DNA samples and elucidating patterns of genetic diversity of the dengue virus (Bennett et al., 2010).

Here, we are interested in estimating effective population size trajectories from gene genealogies. The *effective population size* is an abstract parameter that for a real biological population

is proportional to the rate at which genetic diversity is lost or gained. In the absence of natural selection, the effective population size can be used to approximate census population size by knowing the generation time in calendar units (e.g. years) and the population variability in number of offspring (Wakeley and Sargsyan, 2009). The latter quantity might be difficult to know; however, sometimes it suffices to analyze an arbitrarily rescaled population size trajectory, assuming the variability in number of offspring remains constant. The effective population size is equal to the census population size in an idealized Wright-Fisher model. The Wright-Fisher model is a simple and established model of neutral reproduction in population genetics that assumes random mating and non-overlapping generations. For some RNA viruses, for example human influenza A virus, the effective population size rescaled by generation time (3 to 4 days) cannot be interpreted directly as the effective number of infections because of the presence of strong natural selection. However, one can always adopt a more cautious interpretation of the effective population size as a measure of relative genetic diversity (Rambaut et al., 2008; Frost and Volz, 2010).

Coalescent-based methods for estimation of population size dynamics have evolved from stringent parametric assumptions, such as constant population size or exponential growth (Griffiths and Tavaré, 1994; Kuhner et al., 1998; Drummond et al., 2002), to more flexible nonparametric approaches that assume piecewise linear population trajectories (Strimmer and Pybus, 2001; Ongen-Rhein et al., 2005; Drummond et al., 2005; Heled and Drummond, 2008; Minin et al., 2008). The latter class of methods is more appropriate in the absence of prior knowledge about the underlying demographic dynamics, allowing researchers to infer shapes of population size trajectories rather than to impose parametric constraints on these shapes. These nonparametric methods, however, model population dynamics by imposing *a priori* piecewise continuous functions which require regularization either by smoothing or by controlling the number of change points, also *a priori*. The former regularization – which works better in practice (Minin et al., 2008) – is inherently difficult because these piecewise continuous functions are defined on intervals of varying size. The piecewise nature of these methods creates further modeling problems if one wishes to incorporate covariates into the model or impose constraints on population size dynamics (Minin et al., 2008). In this paper, we propose to solve these problems by bringing the coalescent-based estimation of population dynamics up to speed with modern Bayesian nonparametric methods. Making this leap in statistical methodology will allow us to avoid artificial discretization of population trajectories, to perform regularization without making arbitrary scale choices, and, in the future, to extend our method into a multivariate setting.

Our key insight stems from the fact that the coalescent with variable population size is an inhomogeneous continuous-time Markov chain (Tavaré, 2004) and, therefore, can be viewed as an inhomogeneous point process (Andersen et al., 1995). In fact, all current Bayesian nonparametric methods of estimation of population size dynamics resemble early Bayesian approaches to nonparametric estimation of the Poisson intensity function via piecewise continuous functions (Arjas and Heikkinen, 1997). Estimation of the intensity function of an inhomogeneous Poisson process is a mature field that evolved from maximum likelihood estimation under parametric assumptions (Brillinger, 1979) to frequentist (Diggle, 1985) and, more recently, Bayesian nonparametric methods (Arjas and Heikkinen, 1997; Møller et al., 1998; Kottas and Sansó, 2007; Adams et al., 2009).

Following Adams et al. (2009), we *a priori* assume that population trajectories follow a transformed Gaussian process (GP), allowing us to model the population trajectory as a continuous function. This is a convenient way to specify prior beliefs without a particular functional form on the population trajectory. The drawback of such a flexible prior is that the likelihood func-

tion involves integration over an infinite-dimensional random object and, as a result, likelihood evaluation becomes intractable. Fortunately, we are able to avoid this intractability and perform inference exactly by adopting recent algorithmic developments proposed by Adams et al. (2009). We achieve tractability by a novel data augmentation for the coalescent process that relies on thinning algorithms for simulating the coalescent.

Thinning is an accept/reject algorithm that was first proposed by Lewis and Shedler (1979) for the simulation of inhomogeneous Poisson processes and was later extended to a more general class of point processes by Ogata (1981). In the spirit of Ogata (1981), we develop novel thinning algorithms for the simulation of the coalescent. These algorithms, interesting in their own right, open the door for latent variable representation of the coalescent. This representation leads to a new data augmentation that is computationally tractable and amenable to standard Markov chain Monte Carlo (MCMC) sampling from the posterior distribution of model parameters and latent variables.

We test our method on simulated data and compare its performance with a representative piecewise linear approach, a Gaussian Markov random field (GMRF) based method (Minin et al., 2008). We demonstrate that our method is more accurate and more precise than the GMRF method in all simulation scenarios. We also apply our method to two real data sets that have been previously analyzed in the literature: a hepatitis C virus (HCV) genealogy estimated from sequences sampled in 1993 in Egypt and a genealogy of the H3N2 human influenza A virus estimated from sequences sampled in New York state between 2002 and 2005. In the HCV analysis, we successfully recover all believed key aspects of the population size trajectory. Compared to the GMRF method, our GP method better reflects the uncertainty inherent in the HCV data. In our second real data example, our GP method successfully reconstructs a population trajectory of the human influenza A virus with an expected seasonal series of peaks followed by population bottlenecks, while the GMRF method’s reconstructed trajectory fails to recover some of the peaks and bottlenecks.

2 Methods

2.1 Coalescent Background

The coalescent model allows us to trace the ancestry of a random sample of n genomic sequences. These ancestral relationships are represented by a genealogy or tree; the times at which two sequences or lineages merge into a common ancestor are called coalescent times. The coalescent with variable population size can be viewed as a non-homogeneous Markov death process that starts with n lineages at present time $t_n = 0$ and decreases by one, with time running backwards, until reaching one lineage at t_1 , at which point the samples have been traced to their most recent common ancestor (Griffiths and Tavaré, 1994). Here, we assume that a genealogy with time measured in units of generations is observed. The shape of the genealogy depends on the effective population size trajectory, $N_e(t)$, and the number of samples accumulated through time: the larger the effective population size, the longer two lineages need to wait to meet a common ancestor and the larger the sample size, the faster two lineages coalesce. Formally, let $t_n = 0$ denote the present time when all the n available sequences are sampled (*isochronous coalescent*) and let $t_n = 0 < t_{n-1} < \dots < t_1$ denote the coalescent times of lineages in the genealogy with time going backwards. Then, the

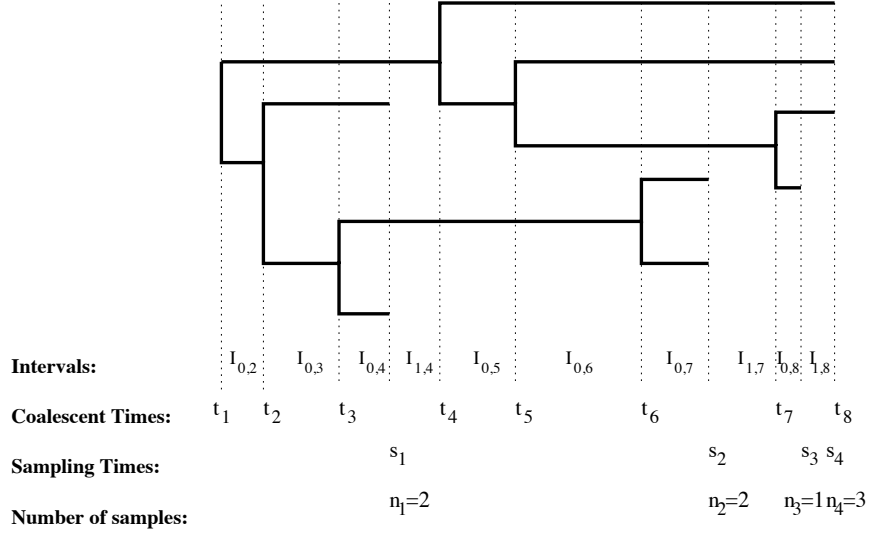


Figure 1: Example of a genealogy relating serially sampled sequences (heterochronous sampling). The number of lineages changes every time we move between intervals ($I_{i,k}$). Each endpoint of an interval is a coalescent time ($\{t_k\}_{k=1}^n$) or a sampling time ($\{s_j\}_{j=1}^m$). The number of sequences sampled at time s_j is denoted by n_j .

conditional density of the coalescent time t_{k-1} takes the following form:

$$P[t_{k-1}|t_k, N_e(t)] = \frac{C_k}{N_e(t_{k-1})} \exp \left\{ - \int_{t_k}^{t_{k-1}} \frac{C_k}{N_e(t)} dt \right\}, \quad (1)$$

where $C_k = \binom{k}{2}$ is the coalescent factor that depends on the number of lineages $k = 2, \dots, n$.

The *heterochronous coalescent* arises when samples of sequences are collected at different times (Figure 1). Such serially sampled data are common in studies of rapidly evolving viruses and analyses of ancient DNA (Campos et al., 2010). Let $t_n = 0 < t_{n-1} < \dots < t_1$ denote the coalescent times as before, but now let $s_m = 0 < s_{m-1} < \dots < s_1 < s_0 = t_1$ denote sampling times of n_m, \dots, n_1 sequences respectively, $\sum_{j=1}^m n_j = n$. Further, let \mathbf{s} and \mathbf{n} denote the vectors of sampling times and numbers of sequences sampled at these times, respectively (Figure 1). Now, the coalescent factor changes not only at the coalescent events but also at the sampling times. Let

$$I_{0,k} = (\max\{t_k, s_j\}, t_{k-1}], \text{ for } s_j < t_{k-1} \text{ and } k = 2, \dots, n, \quad (2)$$

be the intervals that end with a coalescent event and

$$I_{i,k} = (\max\{t_k, s_{j+i}\}, s_{j+i-1}], \text{ for } s_{j+i-1} > t_k \text{ and } s_j < t_{k-1}, k = 2, \dots, n, \quad (3)$$

be the intervals that end with a sampling event. We denote the number of lineages in $I_{i,k}$ with $n_{i,k}$. Then, for $k = 2, \dots, n$,

$$P[t_{k-1}|t_k, \mathbf{s}, \mathbf{n}, N_e(t)] = \frac{C_{0,k}}{N_e(t_{k-1})} \exp - \left\{ \int_{I_{0,k}} \frac{C_{0,k}}{N_e(t)} dt + \sum_{i=1}^m \int_{I_{i,k}} \frac{C_{i,k}}{N_e(t)} dt \right\}, \quad (4)$$

where $C_{i,k} = \binom{n_{i,k}}{2}$. That is, the density for the next coalescent time t_{k-1} is the product of the density of the coalescent time $t_{k-1} \in I_{0,k}$ and the probability of not having a coalescent event during the period of time spanned by intervals $I_{1,k}, \dots, I_{m,k}$ (Felsenstein and Rodrigo, 1999).

2.2 Gaussian Process Prior for Population Size Trajectories

For both isochronous or heterochronous data, we place the same prior on $N_e(t)$:

$$N_e(t) = \left[\frac{\lambda}{1 + \exp\{-f(t)\}} \right]^{-1}, \quad (5)$$

where

$$f(t) \sim \mathcal{GP}(\mathbf{0}, \mathbf{C}(\boldsymbol{\theta})) \quad (6)$$

and $\mathcal{GP}(\mathbf{0}, \mathbf{C}(\boldsymbol{\theta}))$ denotes a Gaussian process with mean function $\mathbf{0}$ and covariance function $\mathbf{C}(\boldsymbol{\theta})$ with hyperparameters $\boldsymbol{\theta}$. *A priori*, $1/N_e(t)$ is a Sigmoidal Gaussian Process, a scaled logistic function of a Gaussian process whose range is restricted to lie in $[0, \lambda]$; λ is a positive constant hyperparameter, the inverse of which serves as a lower bound of $N_e(t)$ (Adams et al., 2009).

A *Gaussian process* is a stochastic process such that any finite sample from the process has a joint Gaussian distribution. The process is completely specified by its mean and covariance functions (Rasmussen and Williams, 2005). For computational convenience we use Brownian motion as our Gaussian process prior. Generating a finite sample from a Gaussian processes requires $\mathcal{O}(n^3)$ computations due to the inversion of the covariance matrix. However, when the precision matrix, the inverse of the covariance, is sparse, such simulations can be accomplished much faster (Rue and Held, 2005). For example, when we choose to work with a Brownian motion with covariance matrix elements $C(t, t') = \frac{1}{\theta}(\min(t, t'))$ and precision parameter θ , then the inverse of this matrix is tri-diagonal, which reduces the computational complexity of simulations from $\mathcal{O}(n^3)$ to $\mathcal{O}(n)$. In our MCMC algorithm, we need to generate realizations from the Gaussian processes at thousands of points, so the speed-up afforded by the Brownian motion becomes almost a necessity, prompting us to use this process as our prior in all our examples.

2.3 Priors for Hyperparameters

The precision parameter θ controls the degree of autocorrelation of our Brownian motion prior and influences the ‘‘smoothness’’ of the reconstructed population size trajectories. We place on θ a Gamma prior distribution with parameters α and β . The other hyperparameter in our model is the upper bound of $1/N_e(t)$, λ . When this upper bound λ is unknown, the model is unidentifiable (see Equation (5)). However, in many circumstances it is possible to obtain an upper bound λ (or equivalently, a lower bound on $N(t)$) from previous studies and use this value to define the prior distribution of λ . We use the following strategy to construct an informative prior for λ . Let $\hat{\lambda}$ denote our best guess of the upper bound, possibly obtained from previous studies. Then, the prior on λ is a mixture of a uniform distribution for values to the left of $\hat{\lambda}$ and an exponential distribution to the right:

$$P(\lambda) = \epsilon \frac{1}{\hat{\lambda}} I_{\{\lambda < \hat{\lambda}\}} + (1 - \epsilon) \frac{1}{\hat{\lambda}} e^{-\frac{1}{\hat{\lambda}}(\lambda - \hat{\lambda})} I_{\{\lambda \geq \hat{\lambda}\}}, \quad (7)$$

where $\epsilon > 0$ is a mixing proportion. When $\hat{\lambda}$ is considerably smaller than the unknown λ , the recovered curve will be visibly truncated around $\hat{\lambda}$, indicating that one needs to try higher values of $\hat{\lambda}$.

2.4 Doubly Intractable Posterior

Coalescent times $\mathcal{T} = \{t_n, t_{n-1}, \dots, t_1\}$ of a given genealogy contain information needed to estimate $N_e(t)$ (see Equations (1) and (4)). Given that $N_e(t)$ is a one-to-one function of $f(t)$ (Equation (5)), we will focus the discussion on the inference of $f(t)$. The posterior distribution of $f(t)$ and hyperparameters θ and λ becomes

$$P(f(t), \theta, \lambda | \mathcal{T}) \propto P(\mathcal{T} | \lambda, f(t)) P(f(t) | \theta) P(\theta) P(\lambda), \quad (8)$$

where $P(f(t) | \theta)$ is a Gaussian process prior with hyperparameter θ and

$$P(\mathcal{T} | \lambda, f(t)) = \prod_{k=2}^n \frac{C_k \lambda}{1 + \exp\{-f(t_{k-1})\}} \exp \left[-C_k \int_{t_k}^{t_{k-1}} \frac{\lambda}{1 + \exp\{-f(t)\}} dt \right] \quad (9)$$

is the likelihood function for the isochronous data (heterochronous data likelihood has a similar form). The integral in the exponent of Equation (9) and the normalizing constant of Equation (8) are computationally intractable, making the posterior doubly intractable (Murray et al., 2006).

Adams et al. (2009) faced a similar doubly intractable posterior distribution in the context of nonparametric estimation of intensity of the inhomogeneous Poisson process. These authors propose an introduction of latent variables so that the augmented data likelihood becomes tractable. This tractability makes the posterior distribution of latent variables and model parameters amenable to standard MCMC algorithms. Since Adams et al. (2009) based their data augmentation on the thinning algorithm for simulating inhomogeneous Poisson processes, we would like to devise a similar data augmentation based on a thinning algorithm for simulation of the coalescent with variable population size. In this simulation, we envision generating coalescent times assuming a constant population size and then thinning these times so that the distribution of the remaining (non-rejected) coalescent times follows the coalescent with variable population size. Since no thinning algorithm for simulating the coalescent process exists, we develop a series of such algorithms. In developing these algorithms, we find it useful to view the coalescent as a point process, a representation that we discuss below.

2.5 The Coalescent as a Point Process

The joint density of coalescent times is obtained by multiplying the conditional densities defined in Equations (1) or (4). This density can be expressed as

$$P(t_1, \dots, t_{n-1} | N_e(t)) = \prod_{k=2}^n \lambda^*(t_{k-1} | t_k) \exp \left\{ - \int_{t_k}^{t_{k-1}} \lambda^*(t | t_k) dt \right\}, \quad (10)$$

where $\lambda^*(t | t_k)$ denotes the conditional intensity function of a point process on the real line (Daley and Vere-Jones, 2002). For isochronous coalescent, the conditional intensity is defined by the step function:

$$\lambda^*(t | t_k) = \binom{k}{2} N_e(t)^{-1} 1_{\{t \in (t_k, t_{k-1}]\}}, \text{ for } k = 2, \dots, n, \quad (11)$$

and the conditional intensity of the heterochronous coalescent point process is:

$$\lambda^*(t | \mathbf{n}, \mathbf{s}, t_k) = \sum_{i=1}^m \binom{n_{i,k}}{2} N_e(t)^{-1} 1_{\{t \in I_{i,k}\}}, \text{ for } k = 2, \dots, n. \quad (12)$$

This novel representation allows us to reduce the task of estimating $N_e(t)$ to the estimation of the inhomogeneous intensity of the coalescent point process and to develop simulation algorithms based on thinning.

2.6 Coalescent Simulation via Thinning

To the best of our knowledge, the only method available for simulating the coalescent under the deterministic variable population size model is a time transformation method (Slatkin and Hudson, 1991; Hein et al., 2005). This method is based on the random time-change theorem due to Pangelou (1972). Under the time transformation method, to simulate coalescent times, we proceed sequentially starting with $k = n$ and $t_n = 0$, generating t from an exponential distribution with unit mean, solving

$$t = \int_{t_k}^{t_{k-1}} \lambda^*(u|t_k) du \quad (13)$$

for t_{k-1} analytically or numerically and repeating the procedure until $k = 2$. For isochronous coalescent, $\lambda^*(u|t_k)$ is defined in Equation (11) and for the heterochronous coalescent, $\lambda^*(u|t_k) = \lambda^*(u|\mathbf{n}, \mathbf{s}, t_k)$ is the piecewise function defined in Equation (12). When $N_e(t)$ is stochastic, the integral in Equation (13) becomes intractable and the time transformation method is no longer practical. Instead, we propose to use *thinning*, a rejection-based method that does not require calculation of the integral in Equation (13).

Lewis and Shedler (1979) proposed thinning a homogeneous Poisson process for the simulation of an inhomogeneous Poisson process with intensity $\lambda(t)$. The idea is to start with a realization of points from a homogeneous Poisson process with intensity λ and accept/reject each point with acceptance probability $\lambda(t)/\lambda$, where $\lambda(t) \leq \lambda$. The collection of accepted points forms a realization of the inhomogeneous Poisson process with conditional intensity $\lambda(t)$. Ogata (1981) extended Lewis and Shedler's thinning for the simulation of any point process that is absolutely continuous with respect to the standard Poisson process. We develop a series of thinning algorithms for the coalescent process that are similar to Ogata's algorithms, but not identical to them. Algorithm 1 outlines the simulation of n coalescent times under the isochronous sampling. Given t_k , we start generating and accumulating exponential random numbers E_i with rate $C_k \lambda$, until $t_{k-1} = t_k + E_1 + E_2 + \dots$ is accepted with probability $1/N_e(t_{k-1})\lambda$. (see Web Appendix A for details and simulation algorithms of coalescent times for heterochronous sampling). In order to ensure convergence of the algorithm, we require $\int_0^\infty \frac{du}{N_e(u)} = \infty$ a.s., which is equivalent to requiring that all sampled lineages can be traced back to their single common ancestor with probability 1. Notice that $N_e(t)$ can be either deterministic or stochastic. The latter case is considered in Web Supplementary Algorithm 2, where we work with $f(t)$ instead of $N_e(t)$ for notational convenience.

If $N_e(t)$ is deterministic and equation (13) can be solved analytically, the time transformation method is likely to be more efficient than thinning since the thinning algorithm is an accept/reject algorithm with the acceptance probability highly dependent on the definition of λ . However, efficiency of the thinning algorithm can be improved by replacing the constant upper bound λ on $1/N_e(t)$, by a piece-wise constant or a piece-wise linear function of local upper bounds in order to achieve higher acceptance probabilities, similarly to the adaptive rejection sampling of Gilks and Wild (1992).

Algorithm 1 Simulation of isochronous coalescent times by thinning - $N_e(t)$ is a deterministic function

Input: $k = n, t_n = 0, t = 0, 1/N_e(t) \leq \lambda, N_e(t)$

Output: $\mathcal{T} = \{t_k\}_{k=1}^n$

- 1: **while** $k > 1$ **do**
 - 2: Sample $E \sim Exponential(C_k \lambda)$ and $U \sim U(0, 1)$
 - 3: $t = t + E$
 - 4: **if** $U \leq \frac{1}{N_e(t)\lambda}$ **then**
 - 5: $k \leftarrow k - 1, t_k \leftarrow t$
 - 6: **end if**
 - 7: **end while**
-

2.7 Data Augmentation and Inference

As mentioned in the previous section, our thinning algorithm for the coalescent is motivated by our desire to construct a data augmentation scheme. We imagine that observed coalescent times \mathcal{T} were generated by the thinning procedure described in Algorithm 1, so we augment \mathcal{T} with rejected (thinned) points \mathcal{N} . If we keep track of the rejected points resulting from Algorithm 1, then, given $t_k, f(t_k), \mathbf{f}_{\mathcal{N}_k} = \{f(t_{k,i})\}_{i=1}^{m_k}$ and λ , we start proposing new time points $\mathcal{N}_k = \{t_{k,1}, \dots, t_{k,m_k}\}$ until t_{k-1} is accepted, so that

$$P(t_{k-1}, \mathcal{N}_k | t_k, f(t_{k-1}), \mathbf{f}_{\mathcal{N}_k}, \lambda) = (C_k \lambda)^{m_k+1} \exp\{-C_k \lambda(t_k - t_{k-1})\} \left[\frac{1}{1 + \exp\{-f(t_{k-1})\}} \right] \times \prod_{i=1}^{m_k} \left[1 - \frac{1}{1 + \exp\{-f(t_{k,i})\}} \right]. \quad (14)$$

For the heterochronous coalescent (see Algorithm 3 in Web Supplemental Materials), Equation (14) is modified in the following way:

$$P(t_{k-1}, \mathcal{N}_k | t_k, f(t_{k-1}), \mathbf{f}_{\mathcal{N}_k}, \lambda, \mathbf{s}, \mathbf{n}) = (\lambda C_{0,k})^{1+m_{0,k}} \exp\{-\lambda C_{0,k} l(I_{0,k})\} \times \left[\left(\frac{1}{1 + \exp\{-f(t_{k-1})\}} \right) \prod_{i=1}^{m_k} \frac{1}{1 + \exp\{f(t_{k,i})\}} \right] \prod_{i=1}^m [(\lambda C_{i,k})^{m_{i,k}} \exp\{-\lambda C_{i,k} l(I_{i,k})\}], \quad (15)$$

where $l(I_{i,k})$ denotes the length of the interval $I_{i,k}$ and $m_{i,k} = \sum_{l=1}^{m_k} 1\{t_{k,l} \in I_{i,k}\}$ denotes the number of latent points in interval $I_{i,k}$. Let $\mathbf{f}_{\mathcal{T}, \mathcal{N}} = \{\{f(t_k)\}_{k=1}^n, \{\{f(t_{k,i})\}_{i=1}^{m_k}\}_{k=2}^n\}$, then the augmented data likelihood of \mathcal{T} and \mathcal{N} becomes

$$P(\mathcal{T}, \mathcal{N} | \mathbf{f}_{\mathcal{T}, \mathcal{N}}, \lambda) = \prod_{k=2}^n P(t_{k-1}, \mathcal{N}_k | t_k, f(t_{k-1}), \mathbf{f}_{\mathcal{N}_k}, \lambda). \quad (16)$$

Then, the posterior distribution of $f(t)$ and hyperparameters evaluated at the observed \mathcal{T} and latent \mathcal{N} time points is

$$P(\mathbf{f}_{\mathcal{T}, \mathcal{N}}, \lambda, \theta | \mathcal{T}, \mathcal{N}) \propto P(\mathcal{T}, \mathcal{N} | \mathbf{f}_{\mathcal{T}, \mathcal{N}}, \lambda) P(\mathbf{f}_{\mathcal{T}, \mathcal{N}} | \theta) P(\lambda) P(\theta). \quad (17)$$

The augmented posterior can now be easily evaluated since it does not involve integration of infinite-dimensional random functions. We follow Adams et al. (2009) and develop a MCMC algorithm

to sample from the posterior distribution (16). At each iteration of our MCMC, we update the following variables: (1) number of “rejected” points $\#\mathcal{N}$; (2) the locations of the rejected points \mathcal{N} ; (3) the function values $\mathbf{f}_{\mathcal{T},\mathcal{N}}$ and (4) the hyperparameters θ and λ . We use a Metropolis-Hastings algorithm to sample the number and locations of latent points and the hyperparameter λ ; we Gibbs sample the hyperparameter θ . Updating the function values $\mathbf{f}_{\mathcal{T},\mathcal{N}}$ is nontrivial, because this high dimensional vector has correlated components. In such cases, single-site updating is inefficient and block updating is preferred (Rue and Held, 2005). We use elliptical slice sampling, proposed by Murray et al. (2010), to sample $\mathbf{f}_{\mathcal{T},\mathcal{N}}$. The advantage of using the elliptical slice sampling proposal is that it does not require the specification of tuning parameters and works well in high dimensions. The details of our MCMC algorithm can be found in Web Appendix B.

We summarize the posterior distribution of $N_e(t)$ by its empirical median and 95% Bayesian credible intervals (BCIs) evaluated at a grid of points. This grid can be made as fine as necessary after the MCMC is finished. That is, given the function values $\mathbf{f}_{\mathcal{T},\mathcal{N}}$ at coalescent and latent time points, and the value of the precision parameter θ at each iteration, we sample the function values at a grid of points $\mathbf{g} = \{g_1, \dots, g_B\}$ from its predictive distribution $\mathbf{f}_{\mathbf{g}} \sim P(\mathbf{f}_{\mathbf{g}}|\mathbf{f}_{\mathcal{T},\mathcal{N}},\theta)$, and evaluate $\{N_e(g_i)\}_{i=1}^B$.

3 Results

3.1 Simulated Data

We simulate three genealogies relating 100 individuals, sampled at the same time $t = 0$ (isochronous sampling) under the following demographic scenarios: 1) constant population size trajectory: $N_e(t) = 1$; 2) exponential growth: $N_e(t) = 25e^{-5t}$; and 3) population expansion followed by a crash: $N_e(t) = e^{4t}1_{\{t \in [0,0.5]\}} + e^{-2t+3}1_{\{t \in (0.5,\infty)\}}$. We compare the posterior median with the truth by the sum of relative errors (SRE):

$$SRE = \sum_{i=1}^K \frac{|\hat{N}_e(s_i) - N_e(s_i)|}{N_e(s_i)}, \quad (18)$$

where $\hat{N}_e(s_i)$ is the estimated trajectory at time s_i with $s_1 = t_1$, the time to the most recent common ancestor and $s_K = t_n = 0$ for any finite K . Similarly, we compute the mean relative width (MRW) of the 95% BCIs defined in the following way:

$$MRW = \sum_{i=1}^K \frac{|\hat{N}_{97.5}(s_i) - \hat{N}_{2.5}(s_i)|}{KN_e(s_i)}. \quad (19)$$

We also compute the percentage of time, the 95% BCIs cover the truth (envelope) in the following way:

$$envelope = \frac{\sum_{i=1}^K I(\hat{N}_{2.5}(s_i) \leq N(s_i) \leq \hat{N}_{97.5}(s_i))}{K}. \quad (20)$$

As a measure of the frequentist coverage, we calculate the percentage of times the truth is completely covered by the 95% BCIs (envelope = 1), by simulating each demographic scenario and performing Bayesian estimation of each such simulation 100 times.

Table 1: Summary of Simulation Results Depicted in Figure 2. SRE is the sum of relative errors as defined in Equation (19), MRW is the mean relative width of the 95% BCI as defined in Equation (20), envelope is calculated as in Equation (21) and variation is calculated as in Equation (22).

Simulations	SRE		MRW		Envelope		Variation		
	GMRF	GP	GMRF	GP	GMRF	GP	GMRF	GP	TRUTH
Constant	50.41	4.15	4.21	0.72	100.0%	100.0%	2.27	0.08	0.00
Exp. growth	47.65	33.60	2.55	2.35	100.0%	100.0%	30.19	52.41	24.80
Expansion/crash	181.88	140.88	10.7	7.26	77.33%	92.0%	5.69	6.94	13.46

We compute the three statistics for the three simulation scenarios for $K = 150$ at equally spaced time points (Table 1). These statistics do not change significantly when we use higher values of K . Additionally, we compute the variation of $\hat{N}_e(t)$ over a regular grid of $K = 150$ points as follows:

$$variation = \sum_{i=1}^{K-1} |\hat{N}_e(s_{i+1}) - \hat{N}_e(s_i)|, \quad (21)$$

For all simulations, we set the mixing parameter ϵ of the prior density for λ (Equation (7)) to $\epsilon = 0.01$. The parameters of the Gamma prior on the GP precision parameter θ were set to $\alpha = \beta = 0.001$. We summarize our posterior inference in Figure 2 and compare our GP method to the GMRF smoothing method (Minin et al., 2008). The effective population trajectory is log transformed and time is measured in units of generations.

For the constant population scenario (first row in Figure 2), the truth (dashed lines) is almost perfectly recovered by the GP method (solid black line) and the 95% BCIs shown as gray shaded areas are remarkably tight. For the exponential growth simulation (second row), the GMRF method recovers the truth better in the right tail, while our GP method recovers it much better in the left tail. The higher variation of the GP reconstruction in the right tail makes this measure higher than for the GMRF reconstruction. Overall, our GP method better recovers the truth in the exponential growth scenario, as evidenced by SREs and MRWs in Table 1. The last row in Figure 2 shows the results for a population that experiences expansion followed by a crash in effective population size. In this case, 95% BCIs of the two methods do not completely cover the true trajectory. While an area near the bottleneck is particularly problematic, the GP method’s envelope is much higher (92%) than the envelope produced by the GMRF method (77.3%), the variation recovered by the GP method is closer to the true variation in all simulation scenarios and in general, in terms of the four statistics employed here, the GP method shows better performance. Results for the GMRF method were obtained using the **BEAST** software (Drummond et al., 2012) with running times ranging from 25 to 40 minutes, while results for the GP method were obtained using **R** with running times ranging from 60 to 180 minutes. Although our GP implementation takes longer, we obtain better performance in a still reasonable amount of time.

Next, we simulate each of the three scenarios 100 times and compute **the four** statistics described before for both methods. The distributions of these statistics are represented by the boxplots depicted in Figure 3. In general, our GP method has smaller SREs, except in the constant case, where the distributions look very similar; smaller MRWs, larger envelopes and variation closer to the truth. Additionally, we calculate the percentage of times, the envelope is 1 as a proxy for frequentist coverage of the 95% BCIs. Since the 95% BCIs are calculated pointwise at 150 equally

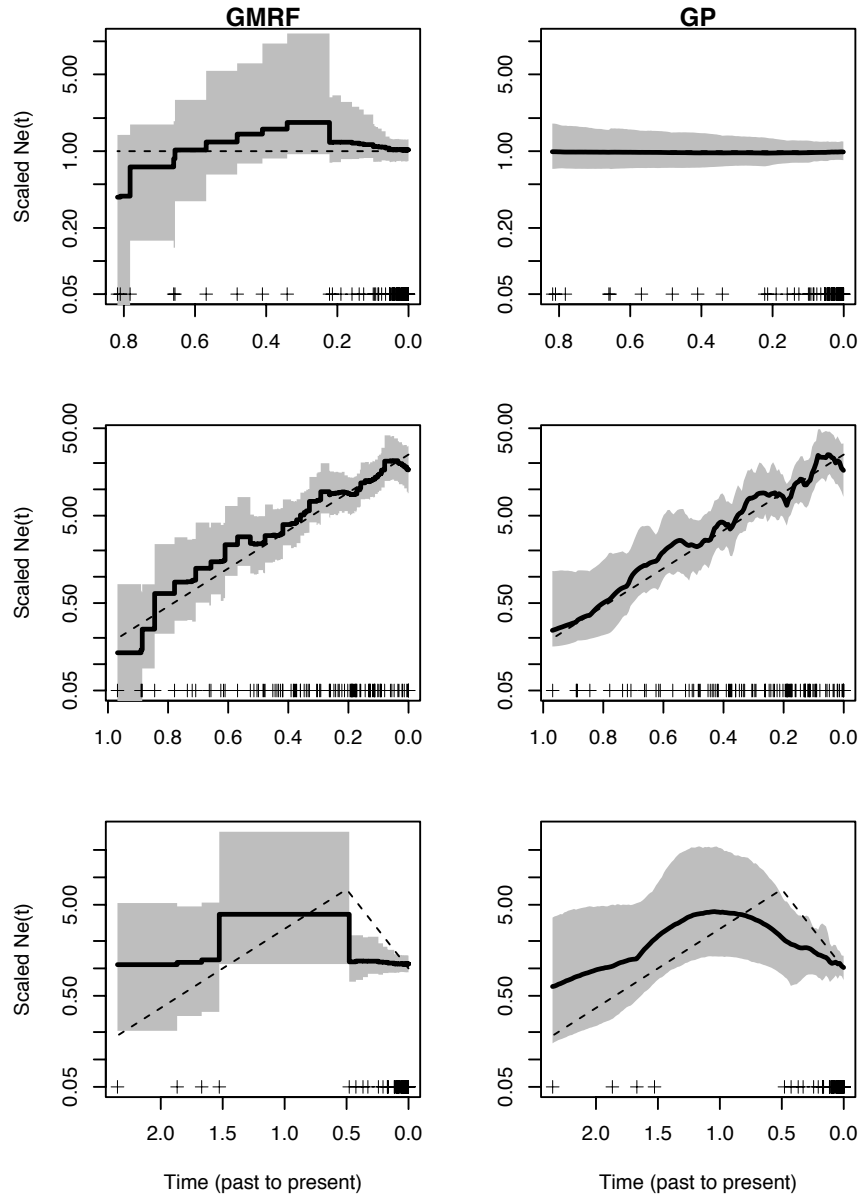


Figure 2: Simulated data under the constant population size (first row), exponential growth (second row) and expansion followed by a crash (third row). The simulated points are represented by the points at the bottom of each plot. We show the log of the effective population size trajectory estimated under the Gaussian Markov random field smoothing (GMRF) method and our method: Gaussian process-based nonparametric inference of effective population size (GP). We show the true trajectories as dashed lines, posterior medians as solid black lines and 95% BCIs by gray shaded areas.

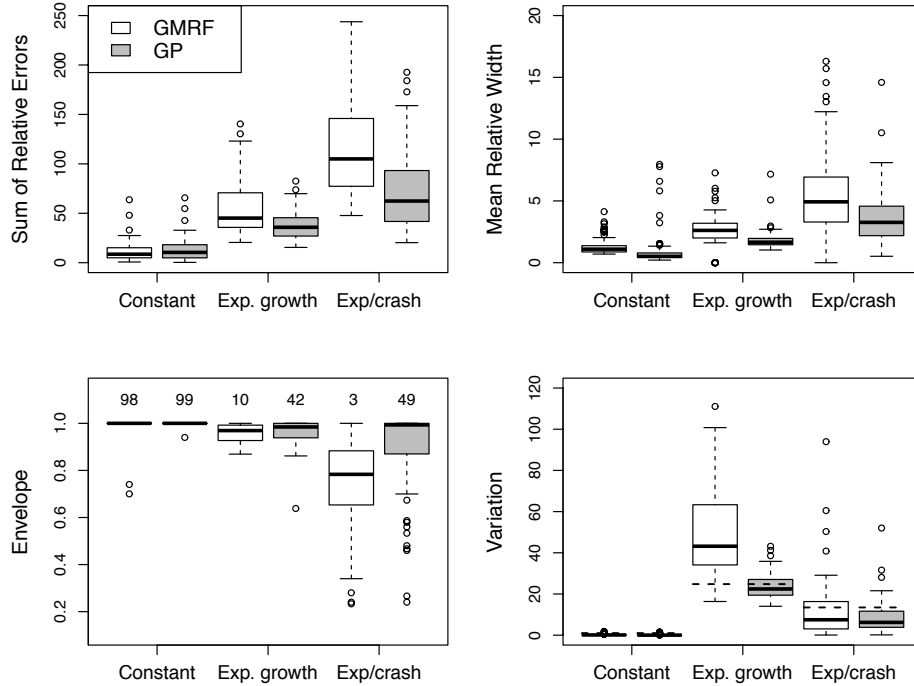


Figure 3: Boxplots of SRE (top left), MRW (top right), envelope (bottom left) and variation (bottom right) based on 100 simulations for a constant trajectory, exponential growth and expansion followed by crash. The numbers above the boxplots of the bottom left plot represent the estimated frequentist coverage of the 95% BCIs, and the dashed lines in the bottom right plot indicate variations of the true simulated trajectories.

spaced points, we do not necessarily expect frequentist coverage to be close to 95%. The results are shown as the numbers at the top of the right plot in Figure 3. The coverage levels obtained using the GP method are larger than those obtained using the GMRF method.

3.2 Egyptian HCV

Hepatitis C virus was first identified in 1989. By 1992, when HCV antibody testing became widely available, the prevalence of HCV in Egypt was about 10.8%. Today, Egypt is the country with the highest HCV prevalence (Miller and Abu-Raddad, 2010). A widely held hypothesis that can explain the epidemic emphasizes the role of a parenteral antischistosomal therapy (PAT) campaign, that started in the 1920s, combined with lack of sanitary practices. The campaign was discontinued in the 1970s when the intravenous treatment was gradually replaced by oral administration of the treatment (Ray et al., 2000). Coalescent demographic methods developed over the last 10 years demonstrated evidence in favor of this hypothesis (Pybus et al., 2003; Drummond et al., 2005; Minin et al., 2008). Therefore, this example is well suited for testing our method. We analyze the genealogy estimated by Minin et al. (2008), based on 63 HCV sequences sampled in Egypt in 1993, and compare our method to the GMRF smoothing method (Minin et al., 2008). The results are depicted in Figure 4, with time scaled in units of years. In line with previous results (Pybus et al., 2003; Drummond et al., 2005; Minin et al., 2008), our estimation recovers the exponential growth of the HCV population size starting from the 1920s when the intravenously administered PAT was introduced. Both Pybus et al. (2003) and Minin et al. (2008) hypothesize that the population

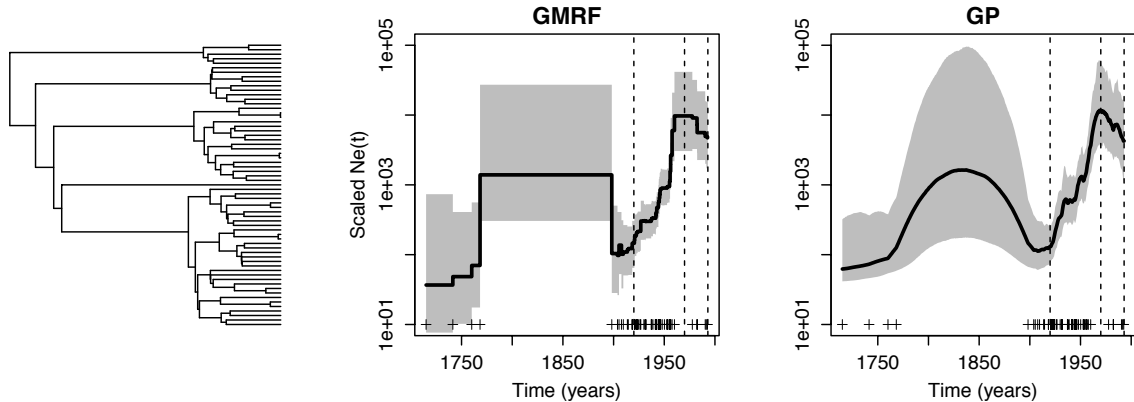


Figure 4: Egyptian HCV. The first plot (left to right) is one possible genealogy reconstructed by Minin et al. (2008). The next two plots represent the log of scaled effective population trajectory estimated using the GMRf smoothing method and our GP method. The posterior medians for the last two plots are represented by solid black lines and the 95% BCI's are represented by the gray shaded areas. The vertical dashed lines mark the years 1920 (the start of intravenous PAT) , 1970 (the end of intravenous PAT) and 1993 (sampling time of sequences).

trajectory remained constant before the start of the exponential growth. The GMRf and GP approaches disagree the most on the HCV population size reconstruction prior to 1920s. The GP method produces narrower BCIs near the root of the genealogy (1710-1770) than the GMRf approach. In contrast, GP BCIs are inflated in the time period from 1770 to 1900 in comparison to the GMRf results. We believe that the uncertainty estimates produced by the GP approach are more reasonable than the GMRf result, because there are multiple coalescent events during 1710- 1770, providing information about the population size, while the time interval 1770 - 1900 has no coalescent events, a data pattern that should result in substantial uncertainty about the HCV population size. Another notable difference between the GMRf and GP methods is in estimation of the HCV population trajectory after 1970. The GP approach suggests a sharper decline in population size during this time interval.

3.3 Seasonal Human Influenza

Here, we estimate population dynamics of human influenza A, based on 288 H3N2 sequences sampled in New York state from January, 2001 to March, 2005. Sequences from the coding region of the influenza hemagglutinin (HA) gene of H3N2 influenza A virus from New York state were collected from the NCBI Influenza Database (Influenza Genome Sequencing Project, 2011), incorporating the exact dates of viral sampling in weeks (heterochronous sampling) and aligned using the software package MUSCLE (Edgar, 2004). These sequences form a subset of sequences analyzed in (Rambaut et al., 2008). We carried out a phylogenetic analysis using the software package BEAST (Drummond et al., 2012) to generate a majority clade support genealogy with median node heights as our genealogical reconstruction. The reconstructed genealogy is depicted in the left plot of Figure 5. Demography of H3N2 influenza A virus in temperate regions, such as New York, is characterized by epidemic peaks during winters followed by strong bottlenecks at the end of epidemic seasons. As expected, our method recovers the peaks in the effective number of infec-

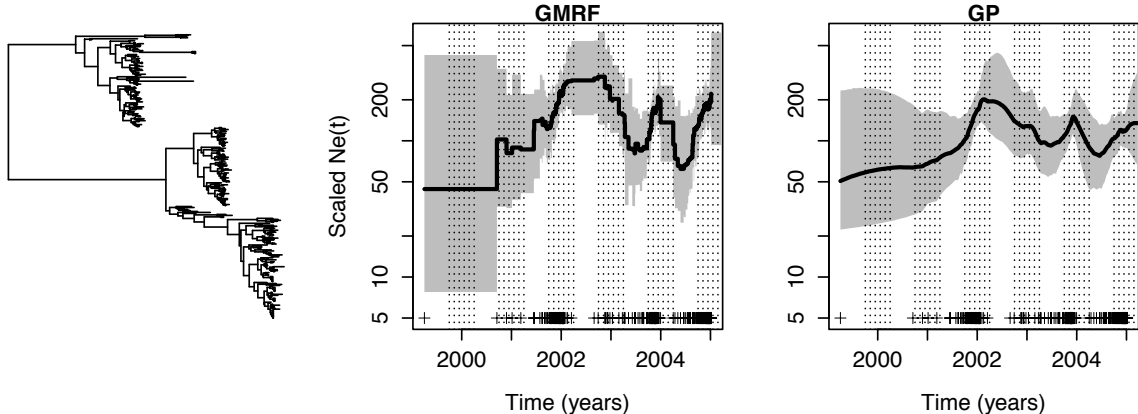


Figure 5: H3N2 Influenza A virus in New York state. The first plot (left) is the estimated genealogy. The second and third plots are the GMRf and GP estimations of log scaled effective population trajectories. Winter seasons are represented by the dotted shaded areas. Posterior medians are represented by solid black lines and 95% BCIs are represented by grey shaded areas.

tions during all seasons starting from the 2001-2002 flu season (flu seasons are represented as dotted rectangles in Figure 5). The GMRf method fails to recover the peak during the 2002-2003 season. The large uncertainty in population size estimation during the 1999-2000, 2000-2001, and at the beginning of 2005-2006 seasons is explained by the small number of coalescent events during those time periods, however, this uncertainty is larger in the GMRf recovered trajectory. During the 2001-2002 flu season, the GMRf method fails to recover the expected trajectory of a peak followed by a bottleneck and instead, this method recovers an epidemic that started during the end of 2001, increased and remained “at peak” until the end of the following winter. The GMRf recovered trajectory during the winter season of 2003 exhibits a steep decrease. In contrast, the GP method detects a late peak during the 2001-2002 season, followed by a decline in the number of infections. There is a small bump in the effective population size of influenza in the winter of 2003, which is more realistic than a steady decline in the number of infections estimated by the GMRf method. Overall, we believe that the GP reconstructed trajectory is more feasible from an epidemiological point of view than the GMRf population size reconstruction.

4 Prior Sensitivity

In all our examples, we placed a Gamma prior on the precision parameter θ with parameters $\alpha = 0.001$ and $\beta = 0.001$. This precision parameter, unknown to us *a priori*, controls the smoothness of the GP prior. We investigate the sensitivity of our results to the Gamma prior specification using the Egyptian HCV data. In the first plot of Figure 6, we show the prior and posterior distributions of θ under our default prior. The difference in densities suggests that prior choices do not have an impact on the posterior distribution. Since the mean of a Gamma distributed random variable is α/β , we investigate the sensitivity by fixing $\beta = .001$ and setting the value of α to 0.001, 0.002, 0.005, 0.01 and 0.1, corresponding to prior means 1, 2, 5, 10 and 100 and variances 1000, 2000, 5000, 10000 and 100000, and by trying two extremes: $\alpha = 1, \beta = .0001$ and $\alpha = .001, \beta = 1$, to examine the posterior distribution of θ under these priors. The posterior sample boxplots displayed

in Figure 6 demonstrate that our results are fairly robust to different choices of α .

5 Sensitivity to the Order of the Gaussian Process

We evaluate our GP-based method for three different Gaussian Process priors for the Egyptian HCV genealogy. In Figure 7, we show the recovered trajectories for Brownian Motion (BM), Ornstein-Uhlenbeck (OU) and approximated Integrated Brownian motion (IBM) (Lindgren and Rue, 2008). The common characteristic of these three priors is the sparsity of their precision matrices (inverse covariance matrix), allowing for computational tractability. Figure 7 shows that the order of the process does make a difference, but only in regions with large posterior uncertainty, where prior influence is more pronounced.

6 Discussion

We propose a new nonparametric method for estimating population size dynamics from gene genealogies. To the best of our knowledge, we are the first to solve this inferential problem using modern tools from Bayesian nonparametrics. In our approach, we assume that the population size trajectory *a priori* follows a transformed Gaussian process. This flexible prior allows us to model population size trajectory as a continuous function without specifying its parametric form and without resorting to artificial discretization methods. We tested our method on simulated and real data and compared it with the competing GMRF method. On simulated data, our method recovers the truth with better accuracy and precision. On real data, where true population trajectories are unknown, our method recovers known epidemiological aspects of the population dynamics and produces more reasonable estimates of uncertainty than the competing GMRF method.

We bring Bayesian nonparametrics into the coalescent framework by viewing the coalescent as a point process. This representation allows us to adapt Bayesian nonparametric methods originally developed for Poisson processes to the coalescent modeling. In particular, it allows us to adapt the thinning-based data augmentation for Poisson processes developed by Adams et al. (2009). We devise an analogous data augmentation for the coalescent by developing a series of new thinning algorithms for the coalescent. Although we use these algorithms in a very narrow context, our novel coalescent simulation protocols should be of interest to a wide range of users of the coalescent. For example, we are not aware of any competitors of our Web Supplementary Algorithms 2 and 4 that allow one to simulate coalescent times with a continuously and *stochastically* varying population size.

Our method works with any Gaussian process with mean $\mathbf{0}$ and covariance matrix \mathbf{C} , where the latter controls the level of smoothness and autocorrelation. For computational tractability however, sparsity in the precision matrix (inverse covariance matrix) may be necessary for complex trajectories with a high number of latent points. One way to achieve sparse matrix computations and computational tractability is to use GP that is also Markov. In all our examples, we use Brownian motion with precision parameter θ ; however, the nondifferentiability characteristic of the Brownian motion is compensated by the fact that our estimate of effective population trajectory is the posterior median evaluated pointwise, which is smoother than any of the sampled posterior curves. Additionally, we compared Brownian motion, Ornstein-Uhlenbeck and a higher order integrated Brownian motion for one of our examples and obtained very similar results under all three priors (see Web Supplementary Materials). Finite sample distributions under these three priors enjoy

sparse precision matrices that yield computational tractability comparable to the GMRF method. In our Brownian motion prior, the precision parameter controls the level of smoothness of the estimated population size trajectory. We find that this important parameter shows little sensitivity to prior perturbations.

Our method assumes that a genealogy or tree is given to the researcher. However, genealogies are themselves inferred from molecular sequences, so we need to incorporate genealogical uncertainty into our estimation. Our framework can be extended to inference from molecular sequences instead of genealogies by introducing another level of hierarchical modeling into our Bayesian framework, similar to the work of Drummond et al. (2005) and Minin et al. (2008). Further, we plan to extend our method to handle molecular sequence data from multiple loci as in (Heled and Drummond, 2008). Finally, we would like to extend our nonparametric estimation into a multivariate setting, so that we can estimate cross correlations between population size trajectories and external time series. Estimating such correlations is a critical problem in molecular epidemiology.

We deliberately adapted the work of Adams et al. (2009) on estimating the intensity function of an inhomogeneous Poisson process, as opposed to alternative ways to attack this estimation problem (Møller et al., 1998; Kottas and Sansó, 2007), to the coalescent. We believe that among the state-of-the-art Bayesian nonparametric methods, our adopted GP-based framework is the most suitable for developing the aforementioned extensions. First, it is straightforward to incorporate external time series data into our method by replacing a univariate GP prior with a multivariate process that evolves the population size trajectory and another variable of interest in a correlated fashion (Teh et al., 2005). Second, the fact that our method does not operate on a fixed grid is critical for relaxing the assumption of a fixed genealogy, because fixing the grid *a priori* is problematic when one starts sampling genealogies, including coalescent times, during MCMC iterations.

Finally, since the coalescent model with varying population size can be viewed as a particular example of an inhomogeneous continuous-time Markov chain, all our mathematical and computational developments are almost directly transferable to this larger class of models. Therefore, our developments potentially have implications for nonparametric estimation of inhomogeneous continuous-time Markov chains with numerous applications.

Acknowledgements

We thank Peter Guttorp, Joe Felsenstein, and Elizabeth Thompson for helpful discussions. VNM was supported by the NSF grant No. DMS-0856099. JAP acknowledges scholarship from CONA-CyT Mexico to pursue her doctoral work.

References

- Adams, R., Murray, I., and MacKay, D. (2009). Tractable nonparametric Bayesian inference in Poisson processes with Gaussian process intensities. In *Proceedings of the 26th International Conference on Machine Learning*, pages 9–16.
- Andersen, P. K., Borgan, O., Gill, R. D., and Keiding, N. (1995). *Statistical Models Based on Counting Processes*. Springer, 2nd edition.

- Arjas, E. and Heikkinen, J. (1997). An algorithm for nonparametric Bayesian estimation of a Poisson intensity. *Computational Statistics*, 12:385–402.
- Bennett, S., Drummond, A., Kapan, D., Suchard, M., Muñoz-Jordán, J., Pybus, O., Holmes, E., and Gubler, D. (2010). Epidemic dynamics revealed in dengue evolution. *Molecular Biology and Evolution*, 27(4):811–818.
- Brillinger, D. R. (1979). Analyzing point processes subjected to random deletions. *Canadian Journal of Statistics*, 7(1):21–27.
- Campos, P. F., Willerslev, E., Sher, A., Orlando, L., Axelsson, E., Tikhonov, A., Aaris Sørensen, K., Greenwood, A. D., Ralf-Dietrich Kahlke, Kosintsev, P., Krakhmalnaya, T., Kuznetsova, T., Lemey, P., MacPhee, R., Norris, C. A., Shepherd, K., and Suchard, M. A. (2010). Ancient DNA analyses exclude humans as the driving force behind late Pleistocene usk ox (*Ovibos moschatus*) population dynamics. *Proceedings of the National Academy of Sciences*, 107(12):5675–5680.
- Daley, D. and Vere-Jones, D. (2002). *An Introduction to the Theory of Point Processes*, volume 1. Springer, 2nd edition.
- Diggle, P. (1985). A kernel method for smoothing point process data. *Journal of the Royal Statistical Society, Series C (Applied Statistics)*, 34(2):138–147.
- Drummond, A. J., Nicholls, G. K., Rodrigo, A. G., and Solomon, W. (2002). Estimating mutation parameters, population history and genealogy simultaneously from temporally spaced sequence data. *Genetics*, 161(3):1307–1320.
- Drummond, A. J., Rambaut, A., Shapiro, B., and Pybus, O. G. (2005). Bayesian coalescent inference of past population dynamics from molecular sequences. *Molecular Biology and Evolution*, 22(5):1185–1192.
- Drummond, A. J., Suchard, M. A., Xie, D., and Rambaut, A. (2012). Bayesian phylogenetics with BEAUti and the BEAST 1.7. *Molecular Biology and Evolution*, 29:1969–1973.
- Edgar, R. C. (2004). MUSCLE: Multiple sequence alignment with high accuracy and high throughput. *Nucleic Acids Research*, 32(5):1792–1797.
- Felsenstein, J. and Rodrigo, A. G. (1999). Coalescent Approaches to HIV Population Genetics. In *The Evolution of HIV*, pages 233–272. Johns Hopkins University Press.
- Frost, S. D. W. and Volz, E. M. (2010). Viral phylodynamics and the search for an ‘effective number of infections’. *Philosophical Transactions of the Royal Society of London. Series B: Biological Sciences*, 365(1548):1879–1890.
- Gilks, W. R. and Wild, P. (1992). Adaptive rejection sampling for Gibbs sampling. *Journal of the Royal Statistical Society. Series C (Applied Statistics)*, 41(2):pp. 337–348.
- Griffiths, R. C. and Tavaré, S. (1994). Sampling theory for neutral alleles in a varying environment. *Philosophical Transactions of the Royal Society of London. Series B, Biological Sciences*, 344(1310):403–410.

- Hein, J., Schierup, M. H., and Wiuf, C. (2005). *Gene Genealogies, Variation and Evolution: A Primer in Coalescent Theory*. Oxford University Press, USA, 1st edition.
- Heled, J. and Drummond, A. (2008). Bayesian inference of population size history from multiple loci. *BMC Evolutionary Biology*, 8(1):1–289.
- Influenza Genome Sequencing Project (2011). <http://www.niaid.nih.gov/labsandresources/resources/dmid/gsc/influenza/Pages/default.aspx>.
- Kingman, J. (1982). The coalescent. *Stochastic Processes and their Applications*, 13(3):235–248.
- Kottas, A. and Sansó, B. (2007). Bayesian mixture modeling for spatial Poisson process intensities, with applications to extreme value analysis. *Journal of Statistical Planning and Inference*, 137:3151–3163.
- Kuhner, M. K., Yamato, J., and Felsenstein, J. (1998). Maximum likelihood estimation of population growth rates based on the coalescent. *Genetics*, 149(1):429–434.
- Lewis, P. and Shedler, G. (1979). Simulation of nonhomogeneous Poisson processes by thinning. *Naval Research Logistics Quarterly*, 26(3):403–413.
- Lindgren, F. and Rue, H. (2008). On the second-order random walk model for irregular locations. *Scandinavian Journal of Statistics*, 35(4):691–700.
- Miller, F. D. and Abu-Raddad, L. J. (2010). Evidence of intense ongoing endemic transmission of hepatitis C virus in Egypt. *Proceedings of the National Academy of Sciences, USA*, 107(33):14757–14762.
- Minin, V. N., Bloomquist, E. W., and Suchard, M. A. (2008). Smooth skyride through a rough skyline: Bayesian coalescent-based inference of population dynamics. *Molecular Biology and Evolution*, 25(7):1459–1471.
- Møller, J., Syversveen, A. R., and Waagepetersen, R. P. (1998). Log Gaussian Cox processes. *Scandinavian Journal of Statistics*, 25(3):451–482.
- Murray, I., Adams, R. P., and MacKay, D. J. (2010). Elliptical slice sampling. In *Proceedings of the 13th International Conference on Artificial Intelligence and Statistics*, volume 9, pages 541–548.
- Murray, I., Ghahramani, Z., and MacKay, D. (2006). MCMC for doubly-intractable distributions. In *Proceedings of the 22nd Annual Conference on Uncertainty in Artificial Intelligence*, pages 359–366.
- Ogata, Y. (1981). On Lewis’ Simulation Method for Point Processes. *IEEE Transactions on Information Theory*, 27(1):23–31.
- Opgen-Rhein, R., Fahrmeir, L., and Strimmer, K. (2005). Inference of demographic history from genealogical trees using reversible jump Markov chain Monte Carlo. *BMC Evolutionary Biology*, 5:1–6.
- Papangelou, F. (1972). Integrability of expected increments of point processes and a related random change of scale. *Transactions of the American Mathematical Society*, 165:483–506.

- Pybus, O. G., Drummond, A. J., Nakano, T., Robertson, B. H., and Rambaut, A. (2003). The epidemiology and iatrogenic transmission of hepatitis C virus in Egypt: A Bayesian coalescent approach. *Molecular Biology and Evolution*, 20(3):381–387.
- Rambaut, A., Pybus, O. G., Nelson, M. I., Viboud, C., Taubenberger, J. K., and Holmes, E. C. (2008). The genomic and epidemiological dynamics of human influenza A virus. *Nature*, 453(7195):615–619.
- Rasmussen, C. E. and Williams, C. K. I. (2005). *Gaussian Processes for Machine Learning*. The MIT Press.
- Ray, S. C., Arthur, R. R., Carella, A., Bukh, J., and Thomas, D. L. (2000). Genetic epidemiology of hepatitis C virus throughout Egypt. *The Journal of Infectious Diseases*, 182(3):pp. 698–707.
- Rosenberg, N. A. and Nordborg, M. (2002). Genealogical trees, coalescent theory and the analysis of genetic polymorphisms. *Nature Reviews Genetics*, 3(5):380–390.
- Rue, H. and Held, L. (2005). *Gaussian Markov Random Fields: Theory and Applications*. Chapman and Hall.
- Slatkin, M. and Hudson, R. R. (1991). Pairwise comparisons of mitochondrial DNA sequences in stable and exponentially growing populations. *Genetics*, 129(2):555–562.
- Strimmer, K. and Pybus, O. G. (2001). Exploring the demographic history of DNA sequences using the generalized skyline plot. *Molecular Biology and Evolution*, 18(12):2298 –2305.
- Tavaré, S. (2004). Part I: Ancestral inference in population genetics. In *Lectures on Probability Theory and Statistics*, volume 1837 of *Lecture Notes in Mathematics*, pages 1–188. Springer Verlag, New York.
- Teh, Y. W., Seeger, M., and Jordan, M. I. (2005). Semiparametric latent factor models. In *Proceedings of the International Workshop on Artificial Intelligence and Statistics*, volume 10, pages 333–340.
- Wakeley, J. and Sargsyan, O. (2009). Extensions of the coalescent effective population size. *Genetics*, 181:341–345.

A Coalescent Simulation Algorithms

Proposition 1. *Algorithm 1 generates $t_n < t_{n-1} < \dots < t_1$, such that*

$$P(t_{k-1} > t|t_k) = \exp \left[- \int_{t_k}^t \frac{C_k dx}{N_e(x)} \right], \quad (\text{A.1})$$

where $N_e(t)$ is known deterministically.

Proof. Let $T_i = t_k + E_1 + \dots + E_i$, where $\{E_i\}_{i=1}^{\infty}$ are iid exponential $Exp(C_k \lambda)$ random numbers. Given t_k , Algorithm 1 generates and accumulates iid exponential random numbers until T_i is accepted with probability $1/\lambda N_e(T_i)$, in which case, T_i is labeled t_{k-1} . Let $N(t_k, t] = \#\{i \geq 1 : t_k < T_i \leq t\}$ denote the number of iid exponential random numbers generated in $(t_k, t]$. Then, $\{N(t_k, t], t > t_k\}$ constitutes a Poisson process with intensity $C_k \lambda$. Then, given $N(t_k, t] = 1$, the conditional density of a point x in $(t_k, t]$ is $1/(t - t_k)$ and the probability of accepting such a point as a coalescent time point with variable population size is $1/\lambda N_e(x)$. Hence

$$P(t_{k-1} \leq t|t_k, N(t_k, t] = 1) = \frac{1}{\lambda(t - t_k)} \int_{t_k}^t \frac{dx}{N_e(x)}, \quad (\text{A.2})$$

and

$$P(t_{k-1} > t|t_k, N(t_k, t] = m) = \left(1 - \frac{1}{\lambda(t - t_k)} \int_{t_k}^t \frac{dx}{N_e(x)} \right)^m. \quad (\text{A.3})$$

Then,

$$\begin{aligned} P(t_{k-1} > t|t_k) &= \sum_{m=1}^{\infty} P(t_{k-1} > t|t_k, N(t_k, t] = m) P(N(t_k, t] = m) \\ &= \sum_{m=1}^{\infty} \left(1 - \frac{1}{\lambda(t - t_k)} \int_{t_k}^t \frac{dx}{N_e(x)} \right)^m \frac{(C_k \lambda(t - t_k))^m \exp[-C_k \lambda(t - t_k)]}{m!} \\ &= \exp[-C_k \lambda(t - t_k)] \sum_{m=1}^{\infty} \frac{\left(C_k \lambda(t - t_k) - C_k \int_{t_k}^t \frac{dt_{k-1}}{N_e(t_{k-1})} \right)^m}{m!} \\ &= \exp \left[- \int_{t_k}^t \frac{C_k dx}{N_e(x)} \right]. \end{aligned}$$

□

Algorithm 3 and 4 are analogous heterochronous versions of Algorithm 1 and 2.

An R implementation of these algorithms is available at

<http://www.stat.washington.edu/people/jpalacio>.

Algorithm 2 Simulation of isochronous coalescent times by thinning with $f(t) \sim \mathcal{GP}(\mathbf{0}, \mathbf{C}(\theta))$

Input: $k = n, t_n = 0, t = 0, i_j = 0, m_j = 0, j = 2, \dots, n, \lambda$

Output: $\mathcal{T} = \{t_k\}_{k=1}^n, \mathcal{N} = \{\{t_{k,i}\}_{i=1}^{m_k}\}_{k=2}^n, \mathbf{f}_{\mathcal{T}, \mathcal{N}}$

```

1: while  $k > 1$  do
2:   Sample  $E \sim \text{Exponential}(C_k \lambda)$  and  $U \sim U(0, 1)$ 
3:    $t = t + E$ 
4:   Sample  $f(t) \sim P(f(t) | \{f(t_l)\}_{l=k}^n, \{\{f(t_{l,i})\}_{i=1}^{m_l}\}_{l=k}^n; \theta)$ 
5:   if  $U \leq \frac{1}{1 + \exp(-f(t))}$  then
6:      $k \leftarrow k - 1, t_k \leftarrow t$ 
7:   else
8:      $i_k \leftarrow i_k + 1, m_k \leftarrow m_k + 1, t_{k,i_k} \leftarrow t$ 
9:   end if
10: end while

```

Algorithm 3 Simulation of heterochronous coalescent by thinning - $N_e(t)$ is a deterministic function

Input: $n_1, n_2, \dots, n_m, s_1, \dots, s_m, 1/N_e(t) \leq \lambda, N_e(t), m$

Output: for $n = \sum_{j=1}^m n_j, \mathcal{T} = \{t_k\}_{k=1}^n$

```

1:  $i = 1, j = n - 1, n = n_1, t = t_n = s_1$ 
2: while  $i < m + 1$  do
3:   Sample  $E \sim \text{Exp}(\binom{n}{2} \lambda)$  and  $U \sim U(0, 1)$ 
4:   if  $U \leq \frac{1}{N_e(t+E)\lambda}$  then
5:     if  $t + E < s_{i+1}$  then
6:        $t_j \leftarrow t \leftarrow t + E$ 
7:        $j \leftarrow j - 1, n \leftarrow n - 1$ 
8:       if  $n > 1$  then
9:         go to 2
10:      else
11:        go to 14
12:      end if
13:    else
14:       $i \leftarrow i + 1, t \leftarrow s_i, n \leftarrow n + n_i$ 
15:    end if
16:  else
17:     $t \leftarrow t + E$ 
18:  end if
19: end while

```

Algorithm 4 Simulation of heterochronous coalescent by thinning with $f(t) \sim \mathcal{GP}(\mathbf{0}, \mathbf{C}(\theta))$

Input: $n_1, n_2, \dots, n_m, s_1 = 0, \dots, s_m, i_j = 0, m_j = 0, j = 2, \dots, n, \lambda, m$

Output: for $n = \sum_{j=1}^m n_j, \mathcal{T} = \{t_k\}_{k=1}^n, \mathcal{N} = \{\{t_{k,i}\}_{i=1}^{m_k}\}_{k=2}^n, \mathbf{f}_{\mathcal{T}, \mathcal{N}}$

```

1:  $i = 1, j = n - 1, n = n_1, t = t_n = s_1$ 
2: while  $i < m + 1$  do
3:   Sample  $E \sim \text{Exp}(\binom{n}{2}\lambda)$  and  $U \sim U(0, 1)$ 
4:   Sample  $f(t + E) \sim P(f(t + E) | \{f(t_l)\}_{l=k}^n, \{\{f(t_{l,i})\}_{i=1}^{m_l}\}_{l=k}^n; \theta)$ 
5:   if  $U \leq \frac{1}{1 + \exp(-f(t + E))}$  then
6:     if  $t + E < s_{i+1}$  then
7:        $t_j \leftarrow t \leftarrow t + E$ 
8:        $j \leftarrow j - 1, n \leftarrow n - 1$ 
9:       if  $n > 1$  then
10:        go to 2
11:      else
12:        go to 14
13:      end if
14:    else
15:       $i \leftarrow i + 1, t \leftarrow s_i, n \leftarrow n + n_i$ 
16:    end if
17:  else
18:    if  $t + E < s_{i+1}$  then
19:       $t_{j+1, i_{j+1}} \leftarrow t + E, i_{j+1} \leftarrow i_{j+1} + 1$ 
20:    end if
21:     $t \leftarrow t + E$ 
22:  end if
23: end while

```

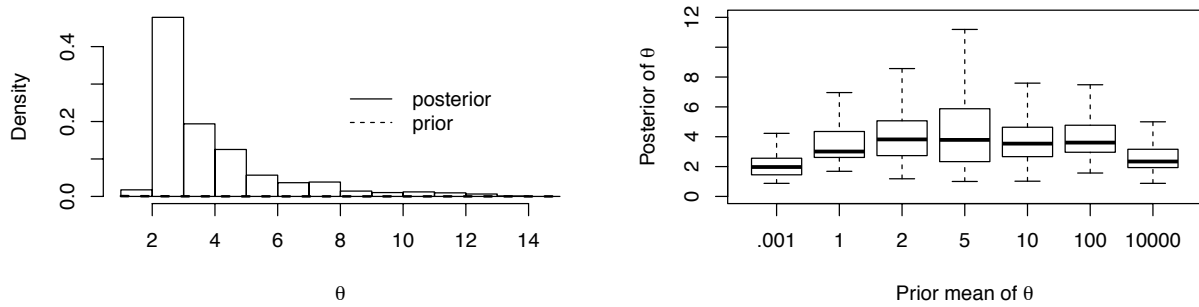


Figure 6: Prior sensitivity on the GP precision parameter. Left plot shows the prior and posterior distributions represented by dashed line and vertical bars respectively. Right plot shows the boxplots of the posterior distributions of the precision parameter when the prior distributions differ in mean and variance of the precision parameter θ . These plots are based on the Egyptian HCV data.

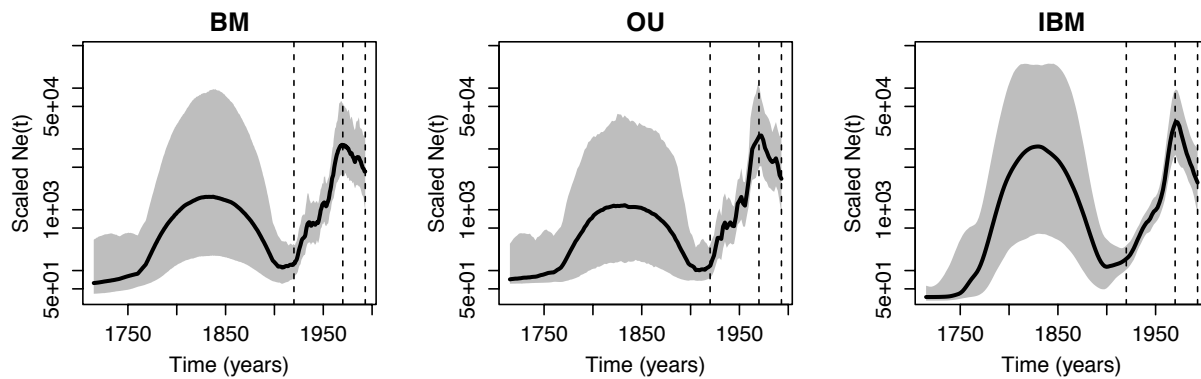


Figure 7: Egyptian HCV recover by placing three different Gaussian process priors. The first plot (left to right) corresponds to a Brownian motion (BM), the second – to Ornstein-Uhlenbeck (OU) and the last one – to the approximated integrated Brownian motion (IBM).

B MCMC Sampling

Since the coalescent under isochronous sampling is a particular case of the coalescent model under heterochronous sampling, we employ here the notation of the heterochronous coalescent, understanding that $C_{0,k} = C_k$, $I_{0,k} = (t_k, t_{k-1}]$ and $i = 0$ for isochronous data.

Sampling the number of latent points. A reversible jump algorithm is constructed for the number of “rejected” points. We propose to add or remove points with equal probability in each interval defined by Equations (3) and (4). When adding a point in a particular interval, we propose a location uniformly from the interval and its predicted function value $f(t^*) \sim P(f(t^*)|\mathbf{f}_{\mathcal{T},\mathcal{N}}, \theta)$. When removing a point, we propose to remove a point selected uniformly from the pool of rejected points in that particular interval. We add points with proposal distributions $q_{up}^{i,k}$ and remove points with proposal distributions $q_{down}^{i,k}$. Then,

$$q_{up}^{i,k} = \frac{P(f(t^*)|\mathcal{T}, \mathcal{N}, \theta)}{2l(I_{i,k})}, \quad (\text{B.1})$$

$$q_{down}^{i,k} = \frac{1}{2m_{i,k}}, \quad (\text{B.2})$$

and the acceptance probabilities are:

$$a_{up}^{i,k} = \frac{l(I_{i,k})\lambda C_{i,k}}{(m_{i,k} + 1)(1 + e^{f(t^*)})}, \quad (\text{B.3})$$

$$a_{down}^{i,k} = \frac{m_{i,k}(1 + e^{f(t^*)})}{l(I_{i,k})\lambda C_{i,k}}. \quad (\text{B.4})$$

Sampling locations of latent points. We use a Metropolis-Hastings algorithm to update the locations of latent points. We first choose an interval defined by Equations (3) and (4) with probability proportional to its length and we then propose point locations uniformly at random in that interval together with their predictive function values $\mathbf{f}_{\mathbf{t}^*} \sim P(\mathbf{f}_{\mathbf{t}^*}|\mathbf{f}_{\mathcal{T},\mathcal{N}}, \theta)$. Since the proposal distributions are symmetric, the acceptance probabilities are:

$$a^{i,k} = \frac{1 + e^{f(t)}}{1 + e^{f(t^*)}}. \quad (\text{B.5})$$

Sampling transformed effective population size values. We use an elliptical slice sampling proposal described in (Murray et al., 2010). In both cases, isochronous or heterochronous, the full conditional distribution of the function values $\mathbf{f}_{\mathcal{T},\mathcal{N}}$ is proportional to the product of a Gaussian density and the thinning acceptance and rejection probabilities:

$$P(\mathbf{f}_{\mathcal{T},\mathcal{N}}|\mathcal{T}, \mathcal{N}, \lambda, \theta) \propto P(\mathbf{f}_{\mathcal{T},\mathcal{N}}|\theta)L(\mathbf{f}_{\mathcal{T},\mathcal{N}}), \quad (\text{B.6})$$

where

$$L(\mathbf{f}_{\mathcal{T},\mathcal{N}}) = \prod_{k=2}^n \left(\frac{1}{1 + e^{-f(t_{k-1})}} \right) \prod_{i=1}^{m_k} \frac{1}{1 + e^{f(t_{k,i})}}. \quad (\text{B.7})$$

Sampling hyperparameters. The full conditional of the precision parameter θ is a Gamma distribution. Therefore, we update θ by drawing from its full conditional:

$$\theta | \mathbf{f}_{\mathcal{T}, \mathcal{N}}, \mathcal{T}, \mathcal{N} \sim \text{Gamma} \left(\alpha^* = \alpha + \frac{\#\{\mathcal{N} \cup \mathcal{T}\}}{2}, \beta^* = \beta + \frac{\mathbf{f}_{\mathcal{T}, \mathcal{N}}^t Q \mathbf{f}_{\mathcal{T}, \mathcal{N}}}{2} \right), \quad (\text{B.8})$$

where $Q = \frac{1}{\theta} C^{-1}$.

For the upper bound λ on $N_e(t)^{-1}$, we use the Metropolis-Hastings update by proposing new values using a uniform proposal reflected at 0. That is, we propose λ^* from $U(\lambda - a, \lambda + a)$. If the proposed value λ^* is negative, we flip its sign. Since the proposal distribution is symmetric, the acceptance probability is:

$$a = \frac{P(\lambda^*)}{P(\lambda)} \left(\frac{\lambda^*}{\lambda} \right)^{\#\{\mathcal{N} \cup \mathcal{T}\}} \exp \left[-(\lambda^* - \lambda) \sum_{k=2}^n \sum_{i=1}^{m_k} C_{i,k} l(I_{i,k}) \right], \quad (\text{B.9})$$

where $P(\lambda)$ is defined in Equation (7).